Study of scattering from a sphere with an eccentrically located spherical inclusion by generalized Lorenz–Mie theory: internal and external field distribution

J. J. Wang,[1,2,*] G. Gouesbet,[2] Y. P. Han,[1] and G. Gréhan[2]

[1]*School of Science, Xidian University, Xi'an, China*
[2]*Laboratoire d'Electromagnétisme des Systèmes Particulaires (LESP), Unité Mixte de Recherche (UMR) 6614 du Centre National de la Recherche Scientifique (CNRS), Complexe de Recherche Interprofessionnel en Aérothermochimie (CORIA), Université de Rouen et Institut National des Sciences Appliquées (INSA) de Rouen BP12, avenue de l'université, technôple du Madrillet, 76801, Saint-Etienne-du Rouvray, France*
**Corresponding author: jiajie.wang@coria.fr.*

Received October 19, 2010; accepted November 11, 2010;
posted November 17, 2010 (Doc. ID 136868); published December 22, 2010

Based on the recent results in the generalized Lorenz–Mie theory, solutions for scattering problems of a sphere with an eccentrically located spherical inclusion illuminated by an arbitrary shaped electromagnetic beam in an arbitrary orientation are obtained. Particular attention is paid to the description and application of an arbitrary shaped beam in an arbitrary orientation to the scattering problem under study. The theoretical formalism is implemented in a homemade computer program written in FORTRAN. Numerical results concerning spatial distributions of both internal and external fields are displayed in different formats in order to properly display exemplifying results. More specifically, as an example, we consider the case of a focused fundamental Gaussian beam (TEM_{00} mode) illuminating a glass sphere (having a real refractive index equal to 1.50) with an eccentrically located spherical water inclusion (having a real refractive index equal to 1.33). Displayed results are for various parameters of the incident electromagnetic beam (incident orientation, beam waist radius, location of the beam waist center) and of the scatterer system (location of the inclusion inside the host sphere and relative diameter of the inclusion to the host sphere).

OCIS codes: 140.0140, 260.2110, 290.0290.

1. INTRODUCTION

The well-known Lorenz–Mie theory (LMT) [1] provides a rigorous way to describe the electromagnetic scattering interaction between a linearly polarized plane wave and a homogeneous spherical particle described by its diameter d and its complex refractive index m. Since the advent of the laser, the interaction of a focused laser beam with different kinds of particles has become a most interesting topic, with applications spread in a variety of fields including particle sizing, Raman scattering diagnostics, optical manipulation, and design of new optics devices. To meet the requirements of these new practical situations, the LMT has been generalized after the name of generalized Lorenz–Mie theory (GLMT) mainly from two perspectives: (i) arbitrary laser beam and (ii) particle shape, with recent reviews by Lock and Gouesbet [2] and by Gouesbet [3]. The GLMT extends the LMT, from the first perspective, to deal with the scattering problem of particles illuminated by an arbitrary laser beam [4–7] instead of a continuous plane wave, which is the case in the LMT framework. Another version to arbitrary shaped beam, equivalent to GLMT, could be found in [8]. The GLMT was also extended to deal with cases of nonspherical and/or composite scatterers from the second perspective, relying on the method of separation of variables (SVM) in various orthogonal coordinate systems [9–12].

For an arbitrary shaped beam, an issue of significance concerns the orientation of the beam with respect to the scatterer. The consideration of arbitrary orientation is compulsory in the case of GLMTs for cylinders and has been implemented, both in circular cylindrical and in elliptical cylindrical coordinates, e.g., [9,13–15] and references therein. In the case of spherical coordinates with spherical particles possessing a complete spherical symmetry (homogeneous spheres, or concentric layered spheres), the concept of arbitrary orientation, more precisely of arbitrary direction (that is to say without accounting for the direction of polarization), is irrelevant since any diameter of the scatterer can be regarded as an axis of symmetry. Any direction of propagation then does belong to the parallel illuminations, including on-axis incident case [16] and off-axis incident case [17]. However, in spherical coordinates, with spherical particles which do not possess a complete spherical symmetry, such as for the case of a spherical particle hosting an eccentric spherical inclusion, we may have to distinguish between parallel and oblique illuminations and relate beam shape coefficients in various coordinate systems obtained, one from the other, by a rotation of coordinates. These issues of oblique illumination and of the transformations of spherical beam shape coefficients through rotations of coordinate systems have been thoroughly investigated recently by us with results that can be found in [18–24]. These recent results obtained in the GLMT framework provide a new tool for the description of illuminating arbitrary beams, including the special case of plane waves, and are implemented in the present paper.

With regard to the shape of the scatterer, the wave scattering problem defined by a host homogeneous sphere embedding an eccentrically located inclusion (or several inclusions) has

attracted much interest in recent years in both electromagnetic- and acoustic-oriented literatures [10,25–30]. This is partially due to the fact that particles or fluid droplets with smaller inclusions are very common in our daily life as well as in the research for industry or environment concerns. For instance, many small particles, such as natural biological spores or cells, possibly artificial biological spores or cells for military purposes, and aerosols in the atmosphere could be regarded as spheres with concentric or eccentric inclusions. Also, fluid droplets with small inclusions such as medicinal sprays or daily cosmetics could be modeled as spherical particles with inclusions as well [31–34].

The associated scattering problem has been studied by using various methods, such as the separation of variables method [10,25], the order of scattering approach [26,27], and the extended boundary condition method (EBCM) [28,35], which is also named null-field method [29]. Nevertheless, most of the previous literature dealt with the case of plane wave illumination. After the introduction of a GLMT for the problem under study by Gouesbet and Gréhan [10], numerical results have been provided by Han *et al.* [36] and Yan *et al.* [37]. Nevertheless, only far-field scattering results were presented in [36,37]. In the present paper, spatial distributions of external and internal fields, including scattered field in the far zone, near-surface field outside of the host sphere and internal field inside the host sphere, are analyzed extensively and systematically by taking advantage of the new aforementioned computational tool [20–24].

One of the purposes of our present work is to cast some light on light-scattering-related experimental or industrial applications such as in particle characterization or identification techniques [31,33,34]. Indeed, as we know, light scattering methods provide ideal means for *in situ* particle characterization or identification, because of their fast responses and nondestructiveness.

Traditionally, light scattering measurements are made with a single, possibly movable, detector, or with a limited number of fixed detectors. Sometimes, such simple facilities might be sufficient due to the inherent symmetries in the scattered field patterns created by particles sharing a high enough level of symmetry, such as spherical particles or axisymmetric particles exhibiting some specific orientations. However, for the study of nonspherical or nonhomogeneous particles, such as the ones investigated in the present paper, in cases where symmetries in the scattered field distribution are broken, more elaborate spatial detections might be required. With improved instrumentation, such as wide application of intensified charge-coupled device cameras, researchers are able to employ two-dimensional angular optical scattering as a tool for analyzing such particle systems [31,38]. Along with the applications of new facilities in the measurements, a knowledge of spatial distributions of the energy intensity is also required in theoretical processing, especially when the symmetry of the scattering pattern is broken, this being an issue that we keep in mind in the present paper.

Another motivation of our study lies on the expected future detection of optical (Hamiltonian) chaos features depicted in [39–41], which might be associated with the destruction and splitting of morphology-dependent resonances (MDRs) [27,42,43]. Such features are associated with the increase of complexity of the optical interactions between the eccentrically located inclusion and the host sphere, generated by a loss of spherical symmetry. The curved surfaces of the particle system together with the discontinuity of the complex refractive index at the interface of two different media influence the spatial distribution of the field intensities both in the internal and external regions. In this paper, spatial distributions of the internal and near-surface fields for the scattering system under study in off-resonance conditions are presented for the first time, with the expectation that the numerical results given here would contribute to the understanding of multiple scattering interactions between closely spaced particles or between different parts of a scattering system.

The body of the present paper is organized as follows. In Section 2, we present a theoretical treatment for the scattering problem of a sphere with an eccentrically located spherical inclusion illuminated by an arbitrary shaped electromagnetic beam in an arbitrary orientation in the framework of GLMT. Particular attention is paid to the description and application of an arbitrary shaped beam in an arbitrary orientation to the problem under study. In Section 3, the case of a focused Gaussian beam in the fundamental mode (TEM_{00}) is specifically considered for numerical illustration. Spatial distributions of both internal and external fields, including scattered field in the far zone, near-surface field outside of the host sphere and internal field inside the host sphere, are presented for various parameters of the incident electromagnetic beam and of the scatterer system. Some discussions are presented in Section 4, which serves as a conclusion as well.

2. THEORETICAL TREATMENT BY GLMT

A. Definition of the Problem

The geometry of the specific scattering problem under study is illustrated in Fig. 1. The host sphere is attached to a global Cartesian coordinate system $(O_1X_1Y_1Z_1)$, and its corresponding spherical coordinates are designated as $(r_1, \theta_1, \varphi_1)$. A spherical inclusion is embedded in the host sphere. It is attached to an inclusion coordinate system $(O_2X_2Y_2Z_2)$, whose corresponding spherical coordinates are designated as $(r_2, \theta_2, \varphi_2)$. The three axes in the inclusion coordinate system

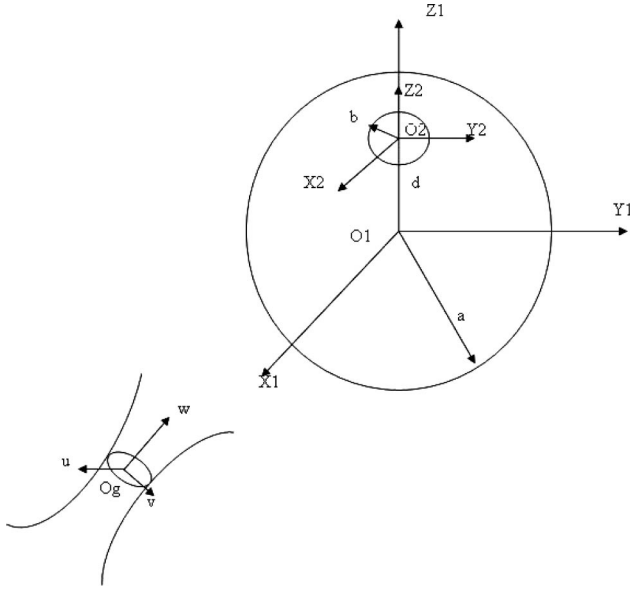

Fig. 1. Scattering geometry of the problem under study.

are parallel to the corresponding axes in the global coordinate system, respectively.

Without any loss of generality, the center of the inclusion is located on the z axis of the global coordinate system. The center–center separation distance is designated by d; we have

$$x_2 = x_1, \qquad y_2 = y_1, \qquad z_2 = z_1 - d. \tag{1}$$

The radii of the host sphere and of the inclusion are a and b, respectively. The complex refractive index and wavenumber of the surrounding medium are m_0 and k_0, the corresponding parameters for the host sphere are m_1 and k_1, and for the inclusion, m_2 and k_2.

The scattering model in Fig. 1 is illuminated by an arbitrary shaped beam propagating along the w axis in the beam coordinate system O_gUVW. The coordinates of its origin O_g with respect to the global coordinate system $(O_1X_1Y_1Z_1)$ are denoted as (x_0, y_0, z_0). The frame system $(O_1X_1Y_1Z_1)$ can be obtained from the beam coordinate system (O_gUVW) by rotations through Euler angles (α, β, γ) [20–23] followed by a translation of (x_0, y_0, z_0), and vice versa. In this paper, a focused Gaussian beam propagating along the w axis with beam waist center located in the origin of the beam coordinate system O_gUVW is specified for numerical illustration. The time-dependence factor reading as $\exp(jwt)$ is assumed, where w is the angular frequency. This term will be omitted from all formulas for the sake of conciseness.

B. Vector Spherical Wave Functions

The vector spherical wave functions (VSWFs) used in this paper are a little different from the ones used in [20,44] by a normalization factor and also by the fact that we have interchanged the indices n and m, i.e., $\mathbf{M}_{nm}^{(j)}$ instead of $\mathbf{M}_{mn}^{(j)}$ and similarly for $\mathbf{N}_{nm}^{(j)}$. Nevertheless, the interchanges of orders n and m in subscripts occur only superficially in appearance for the purpose of consistency in the paper, which will not change their original meanings. They read as

$$\mathbf{M}_{nm}^{(j)} = (-1)^m [im\tilde{\pi}_n^m(\cos\theta)\mathbf{i}_\theta - \tilde{\tau}_n^m(\cos\theta)\mathbf{i}_\varphi] z_n(kr)\exp(im\varphi), \tag{2}$$

$$\begin{aligned}\mathbf{N}_{nm}^{(j)} = (-1)^m \Bigg\{ & \frac{n(n+1)}{kr} z_n(kr)\tilde{P}_n^m(\cos\theta)\mathbf{i}_r \\ & + \frac{1}{kr}\left[\frac{d}{dr} r z_n(kr)\right]\tilde{\tau}_n^m(\cos\theta)\mathbf{i}_\theta \\ & + \frac{1}{kr}\left[\frac{d}{dr} r z_n(kr)\right] im\tilde{\pi}_n^m(\cos\theta)\mathbf{i}_\varphi \Bigg\} \exp(im\varphi),\end{aligned} \tag{3}$$

in which $\mathbf{i}_r$, $\mathbf{i}_\theta$, and $\mathbf{i}_\varphi$ are standard unit vectors associated with the coordinates r, θ, and φ, respectively, of a spherical coordinate system (r, θ, φ), k is the wavenumber in the considered medium, $z_n(kr)$ designates any spherical Bessel function $(j_n, y_n, h_n^{(1)}, h_n^{(2)})$, and $\tilde{\pi}_n^m$ and $\tilde{\tau}_n^m$ designate the normalized generalized Legendre functions according to

$$\tilde{\pi}_n^m(\cos\theta) = \frac{\tilde{P}_n^m(\cos\theta)}{\sin\theta}; \qquad \tilde{\tau}_n^m(\cos\theta) = \frac{d}{d\theta}\tilde{P}_n^m(\cos\theta). \tag{4}$$

$\tilde{P}_n^m(\cos\theta)$ is the fully normalized associated Legendre function, which is normalized from the associated Legendre functions $P_n^m(\cos\theta)$:

$$\tilde{P}_n^m(\cos\theta) = c_n^m P_n^m(\cos\theta), \tag{5}$$

where c_n^m is a normalization factor:

$$c_n^m = (-1)^m \sqrt{\frac{2n+1}{2}\frac{(n-m)!}{(n+m)!}}, \tag{6}$$

and the associated Legendre functions $P_n^m(\cos\theta)$ read as

$$P_n^m(\cos\theta) = (-1)^m(\sin\theta)^m \frac{d^m P_n(\cos\theta)}{(d\cos\theta)^m}. \tag{7}$$

C. Solutions

The theoretical treatment to scattering from a sphere with an eccentrically located spherical inclusion illuminated by an arbitrary shaped beam was originally presented by Gouesbet and Gréhan [10]. Afterward, Han *et al.* [36] and Yan *et al.* [37] also studied this problem. Here, we will not focus on these derivations but recall some expressions necessary for the sequel.

In the global coordinate system, an arbitrary shaped beam in an arbitrary orientation illuminating the host sphere may be expressed in terms of VSWFs with two sets of expansion coefficients a_{nm} and b_{nm}:

$$\mathbf{E}^{\text{inc}} = \sum_{n=1}^{\infty}\sum_{m=-n}^{+n} a_{nm}\mathbf{M}_{nm}^{(1)}(k_0\mathbf{r}_1) + b_{nm}\mathbf{N}_{nm}^{(1)}(k_0\mathbf{r}_1), \tag{8}$$

in which the field strength E_0 has been set equal to unity. Furthermore, the relationship between the expansion coefficients a_{nm} and b_{nm} on one hand and the more traditional beam shape coefficients g_{nX}^m on the other hand is available from [44] and will be provided in the sequel.

Similarly, the scattered field may be expanded using the spherical Bessel functions of the fourth kind:

$$\mathbf{E}^{\text{sca}} = \sum_{n=1}^{\infty}\sum_{m=-n}^{+n} c_{nm}\mathbf{M}_{nm}^{(4)}(k_0\mathbf{r}_1) + d_{nm}\mathbf{N}_{nm}^{(4)}(k_0\mathbf{r}_1). \tag{9}$$

The main field in the annular zone between the surface of the host sphere and that of the inclusion may be expressed using the spherical Bessel functions of the third and the fourth kind in the global coordinates system, indicating a superposition of incoming and outcoming partial waves:

$$\begin{aligned}\mathbf{E}^{\text{int1}} = \sum_{n=1}^{\infty}\sum_{m=-n}^{+n} & e_{nm}\mathbf{M}_{nm}^{(3)}(k_1\mathbf{r}_1) + f_{nm}\mathbf{N}_{nm}^{(3)}(k_1\mathbf{r}_1) \\ & + v_{nm}\mathbf{M}_{nm}^{(4)}(k_1\mathbf{r}_1) + h_{nm}\mathbf{N}_{nm}^{(4)}(k_1\mathbf{r}_1).\end{aligned} \tag{10}$$

In [10], Eqs. (11) and (12), the choice has been made to use the first and fourth kinds of VSWFs instead , indicating superposition of waves incident on the inclusion and of waves scattered from the inclusion.

The incident coefficients a_{nm} and b_{nm} and the scattered coefficients c_{nm} and d_{nm} can then be related to the expansion coefficients e_{nm}, f_{nm}, v_{nm}, and h_{nm} by applying the

well-known boundary conditions at the main sphere surface $r_1 = a$, according to which the tangential components of the electric and magnetic field would be continuous across the sphere surface.

The same procedure is then implemented in the inclusion coordinate system, which relates the expansion coefficients r_{nm}, s_{nm}, t_{nm}, and u_{nm} of the main field,

$$\mathbf{E}^{\text{int1}} = \sum_{n=1}^{\infty}\sum_{m=-n}^{+n} r_{nm}\mathbf{M}_{nm}^{(3)}(k_1\mathbf{r}_2) + s_{nm}\mathbf{N}_{nm}^{(3)}(k_1\mathbf{r}_2) + t_{nm}\mathbf{M}_{nm}^{(4)}(k_1\mathbf{r}_2) + u_{nm}\mathbf{N}_{nm}^{(4)}(k_1\mathbf{r}_2), \tag{11}$$

to the expansion coefficients p_{nm}, and q_{nm} of the internal field inside the inclusion,

$$\mathbf{E}^{\text{int2}} = \sum_{n=1}^{\infty}\sum_{m=-n}^{+n} p_{nm}\mathbf{M}_{nm}^{(1)}(k_2\mathbf{r}_2) + q_{nm}\mathbf{N}_{nm}^{(1)}(k_2\mathbf{r}_2), \tag{12}$$

by applying the well-known boundary conditions at the inclusion surface $r_2 = b$.

In order to obtain the solutions to the scattering problem, translational addition theorems of VSWFs [45,46] should be applied to the main field so as to relate its expansion coefficients e_{nm}, f_{nm}, v_{nm}, andh_{nm} in the global coordinate system with those r_{nm}, s_{nm}, t_{nm}, and u_{nm} in the inclusion coordinate system. Relevant translational coefficients of the vector addition theorem as well as those of the scalar addition theorem have been discussed in the literature, e.g., [29,47,48], and are given in Appendix A.

As a summary, in the global coordinate system, the expansion coefficients that describe the scattered field, c_{nm} and d_{nm}, and the expansion coefficients that describe the main field, e_{nm}, f_{nm}, v_{nm}, and h_{nm}, can be related to the expansion coefficients that describe the incident field a_{nm} and b_{nm} by application of the boundary conditions, according to which the tangential components of the electric and magnetic field would be continuous across the sphere surface. Similarly, in the inclusion coordinate system, the expansion coefficients which describe the inclusion internal field, p_{nm} and q_{nm}, can be related to the expansion coefficients describing the main field, r_{nm}, s_{nm}, t_{nm}, and u_{nm}, by application of the corresponding boundary conditions at the surface of the spherical inclusion. The solutions to the scattering problem can then be readily reached by applying translational addition theorems of VSWFs to the main field; see [10] for details.

D. Beam Shape Coefficients for an Arbitrary Shaped Beam in an Arbitrary Orientation

In the GLMT, the electromagnetic components of the illuminating beam are described by multipole expansions over a set of basis functions. The expansion coefficients are expressed versus fundamental coefficients, usually denoted as $g_{n,X}^m$ (X is TE, transverse electric, or TM, transverse magnetic, with n from 1 to ∞, m from $-n$ to n), known as beam shape coefficients (BSCs). These BSCs are used to express electromagnetic fields of laser beams in expanded forms, for use in GLMTs, or in other light scattering approaches such as the EBCM. Their calculations form the key issue, and the most difficult one, when dealing with a GLMT. Initiated by Han *et al.* [18,19], a systematic analysis was made recently concerning the transformation of BSCs through rotations of coordinate systems, and corresponding results are published in a series of papers [20–24], providing us a new tool for further studies, especially in cases of nonspherical or composite scatterers.

The relationships between the expansion coefficients a_{nm}, b_{nm} on one hand, and the BSCs $\tilde{g}_{n,X}^m$ on the other hand read as [44]

$$a_{nm} = -ikc_n^{pw}(-1)^m(-1)^{\frac{m-|m|}{2}}\frac{(n-m)!}{(n-|m|)!}\frac{\tilde{g}_{n,\text{TE}}^m}{c_n^m}, \tag{13}$$

$$b_{nm} = kc_n^{pw}(-1)^m(-1)^{\frac{m-|m|}{2}}\frac{(n-m)!}{(n-|m|)!}\frac{\tilde{g}_{n,\text{TM}}^m}{c_n^m}, \tag{14}$$

in which c_n^{pw} are plane wave coefficients reading as [4]

$$c_n^{pw} = \frac{1}{k}(-i)^{n+1}\frac{2n+1}{n(n+1)}. \tag{15}$$

With respect to the corresponding equations in [44], the following modifications have been introduced: (i) the field strength E_0 has again been set equal to unity, (ii) the coefficient c_n^m has been introduced as a consequence of the fact that we use a slightly different definition for the VSWFs [see Subsection 2.B], and (iii) the BSCs are tilde-decorated to indicate that they are valid in a rotated system.

According to the transformation theorem for BSCs in spherical coordinates [20], the tilde-decorated BSCs $\tilde{g}_{n,X}^m$ in a rotated system are expressed versus the BSCs $g_{n,X}^m$ in another system, called the unrotated system, as

$$\tilde{g}_{n,X}^m = \mu_{nm}\sum_{s=-n}^{n}\frac{H_{sn}^m}{\mu_{ns}}g_{n,X}^s, \tag{16}$$

where

$$\mu_{nm} = (-1)^m(-1)^{\frac{m-|m|}{2}}\frac{(n-|m|)!}{(n-m)!}, \tag{17}$$

$$H_{sn}^m = (-1)^{n+s}\frac{(n-m)!}{(n-s)!}e^{im\gamma}e^{is\alpha}\sum_{\sigma}(-1)^{\sigma}\binom{n+s}{n-m-\sigma}\binom{n-s}{\sigma} \times\left(\cos\frac{\beta}{2}\right)^{2\sigma+m+s}\left(\sin\frac{\beta}{2}\right)^{2n-2\sigma-m-s}, \tag{18}$$

in which (α, β, γ) are Euler angles bringing the unrotated system to the rotated system, whose definitions could be found in any of the references [20–24].

With decades of efforts devoted to the description of an arbitrary shaped beam, the BSCs of an arbitrary shaped beam in the unrotated coordinate system can be evaluated by several methods, sharing various degrees of time running efficiency, or of flexibility, namely by using quadratures [49], finite series [50], localized approximations generating localized beam models [6], or by a hybrid method taking advantage of both quadratures and of a localized approximation, named the integral localized approximation [51]. The evaluation of BSCs has also been investigated by relying on addition theorems for translations of coordinate systems, an approach originally introduced by Doicu and Wriedt [52] and also used by Zhang and Han [53]. In our computer program, the Modified Localized Approximation method [6,54], which was rigorously justified by Gouesbet

and Lock [16,17], is applied to evaluate the BSCs in the unrotated coordinate system due to the fact that it provides the most efficient method, with regard to computational times, by orders of magnitude with respect to other methods, such as by using quadratures [55]. It is also the most appealing from a physical point of view because it provides many physical insights on the interpretation of beam models.

In order to describe an arbitrary shaped beam in an arbitrary orientation, the BSCs in the rotated coordinate system have to be evaluated.

Two different ways have been explored to deal with the use of a localization procedure associated with a rotation, namely, a rotation–localization (RL) procedure in which we first apply a localization operator and afterward rotate, and a localization–rotation procedure, in which we first rotate and afterward apply a localization procedure, with details presented in [24]. It has been surprising to uncover that the operations of rotation and localization do not commute, not only for non-Maxwellian beams, but also for Maxwellian beams, in particular, for even a plane wave. Therefore, at the present time, in order to obtain a localized beam model under an arbitrary orientation, one has to use the RL procedure as we have used in this paper. That is to say, after obtaining the BSCs of an arbitrary shaped beam in the unrotated coordinate system by the Modified Localized Approximation method [6,16,17,54], the transformation theorem for BSCs [20–24] is applied to obtain a localized beam model in a rotated system in terms of the localized beam model in the unrotated system.

E. External Near-Surface and Internal Fields

Even though the magnitude and the phase for each component of the electromagnetic field can be determined from the GLMT formalism discussed in this paper, a useful visualization of the electromagnetic field distribution can be obtained by plotting the normalized source function as a function of spatial position. The normalized source function is defined as

$$S = |\mathbf{E}|^2/|E_0|^2, \tag{19}$$

where $\mathbf{E}$ is the electric (internal or external) field and E_0 is the electric field strength of the incident field, which is assumed to be unity in this paper.

1. Internal Field

Inserting Eqs. (2) and (3) into Eq. (11), expressions for evaluating the main internal field in the annular area can be obtained:

$$\mathbf{E}_r^{\mathrm{int1}} = \sum_{n=1}^{\infty}\sum_{m=-n}^{+n}(-1)^m[s_{nm}h_n^{(1)}(k_1r_2) + u_{nm}h_n^{(2)}(k_1r_2)] \times \frac{n(n+1)}{k_1r_2}\tilde{P}_n^m(\cos\theta)\exp(im\varphi), \tag{20}$$

$$\mathbf{E}_\theta^{\mathrm{int1}} = \sum_{n=1}^{\infty}\sum_{m=-n}^{+n}(-1)^m\left\{[r_{nm}h_n^{(1)}(k_1r_2) + t_{nm}h_n^{(2)}(k_1r_2)]im\tilde{\pi}_n^m \times(\cos\theta) + \frac{1}{k_1r_2}\left[s_{nm}\frac{d(r_2h_n^{(1)}(k_1r_2))}{dr_2} + u_{nm}\frac{d(r_2h_n^{(2)}(k_1r_2))}{dr_2}\right]\tilde{\tau}_n^m(\cos\theta)\right\}\exp(im\varphi), \tag{21}$$

$$\mathbf{E}_\varphi^{\mathrm{int1}} = \sum_{n=1}^{\infty}\sum_{m=-n}^{+n}(-1)^m\left\{[-r_{nm}h_n^{(1)}(k_1r_2) - t_{nm}h_n^{(2)}(k_1r_2)]\tilde{\tau}_n^m \times(\cos\theta) + \frac{1}{k_1r_2}\left[s_{nm}\frac{d(r_2h_n^{(1)}(k_1r_2))}{dr_2} + u_{nm}\frac{d(r_2h_n^{(2)}(k_1r_2))}{dr_2}\right]im\tilde{\pi}_n^m(\cos\theta)\right\}\exp(im\varphi). \tag{22}$$

Similarly, the main internal field could also be evaluated in the global coordinate system by using Eq. (10).

Also, the expressions for calculating the internal field inside the inclusion can be obtained:

$$\mathbf{E}_r^{\mathrm{int1}} = \sum_{n=1}^{\infty}\sum_{m=-n}^{+n}(-1)^m q_{nm}\frac{j_n(k_2r_2)}{k_2r_2}n(n+1)\tilde{P}_n^m(\cos\theta)\exp(im\varphi), \tag{23}$$

$$\mathbf{E}_\theta^{\mathrm{int1}} = \sum_{n=1}^{\infty}\sum_{m=-n}^{+n}(-1)^m\left\{p_{nm}j_n(k_2r_2)im\tilde{\pi}_n^m(\cos\theta) + q_{nm}\frac{1}{k_2r_2}\frac{d(r_2j_n(k_2r_2))}{dr_2}\tilde{\tau}_n^m(\cos\theta)\right\}\exp(im\varphi), \tag{24}$$

$$\mathbf{E}_\varphi^{\mathrm{int1}} = \sum_{n=1}^{\infty}\sum_{m=-n}^{+n}(-1)^m\left\{-p_{nm}j_n(k_2r_2)\tilde{\tau}_n^m(\cos\theta) + q_{nm}\frac{1}{k_2r_2}\frac{d(r_2j_n(k_2r_2))}{dr_2}im\tilde{\pi}_n^m(\cos\theta)\right\}\exp(im\varphi). \tag{25}$$

2. External Near-Surface Field

The external near-surface field is a summation of the incident field and the scattered field. The intensity of the incident shaped beam can be evaluated either by using analytical expressions in closed form (see [4]) or by using expressions in expanded form from Eq. (8), which is applied in our simulations in this paper. The approach for calculations of the scattered field in the near zone is very similar to that used in the calculation of the internal field. The only significant difference lies in the number of summation terms. In the evaluation of scattered field, the number of terms taken into account is fixed at a cut-off number related with the size parameter of the host sphere. While in the evaluation of internal intensity distribution, a fewer number of summation terms for smaller radii than the fixed cut-off number have to be taken into account.

The expressions for calculating the scattered field in the near zone are given:

$$\mathbf{E}_r^{\mathrm{sca}} = \sum_{n=1}^{\infty}\sum_{m=-n}^{+n}(-1)^m d_{nm}\frac{h_n^{(2)}(k_0r_1)}{k_0r_1}n(n+1)\tilde{P}_n^m(\cos\theta) \times\exp(im\varphi), \tag{26}$$

$$\mathbf{E}_\theta^{\mathrm{sca}} = \sum_{n=1}^{\infty}\sum_{m=-n}^{+n}(-1)^m\left\{c_{nm}h_n^{(2)}(k_0r_1)im\tilde{\pi}_n^m(\cos\theta) + d_{nm}\frac{1}{k_0r_1}\frac{d(r_1h_n^{(2)}(k_0r_1))}{dr_1}\tilde{\tau}_n^m(\cos\theta)\right\}\exp(im\varphi), \tag{27}$$

$$\mathbf{E}_{\varphi}^{\mathrm{sca}} = \sum_{n=1}^{\infty}\sum_{m=-n}^{+n}(-1)^m\left\{-c_{nm}h_n^{(2)}(k_0r_1)\tilde{\tau}_n^m(\cos\theta) + d_{nm}\frac{1}{k_0r_1} \times \frac{d(r_1h_n^{(2)}(k_0r_1))}{dr_1}im\tilde{\pi}_n^m(\cos\theta)\right\}\exp(im\varphi). \quad (28)$$

F. Scattered Field in the Far Zone

In the far zone away from the scatterer, where $kr \gg ka$, the spherical Hankel functions reduce to spherical waves, according to

$$h_n^{(2)}(kr) \sim i^{n+1}\frac{e^{-ikr}}{kr}, \qquad \frac{dh_n^{(2)}(kr)}{d(kr)} \sim i^n\frac{e^{-ikr}}{kr}. \quad (29)$$

Inserting Eq. (29) into Eq. (26)–(28), the scattered field in the far zone degenerates to transversal spherical waves, and the nonzero components are expressed as

$$\mathbf{E}_{\theta}^{\mathrm{sca}} = i\frac{e^{-ik_0r_1}}{k_0r_1}\sum_{n=1}^{\infty}\sum_{m=-n}^{+n}[c_{nm}m\tilde{\pi}_n^m(\cos\theta) - d_{nm}\tilde{\tau}_n^m(\cos\theta)]i^{n+1}(-1)^m\exp(im\varphi), \quad (30)$$

$$\mathbf{E}_{\varphi}^{\mathrm{sca}} = \frac{e^{-ik_0r_1}}{k_0r_1}\sum_{n=1}^{\infty}\sum_{m=-n}^{+n}[-c_{nm}\tilde{\tau}_n^m(\cos\theta) + d_{nm}m\tilde{\pi}_n^m(\cos\theta)]i^{n+1}(-1)^m\exp(im\varphi). \quad (31)$$

The scattering intensity may be expressed as [4]

$$\begin{pmatrix} I_{\theta} \\ I_{\varphi} \end{pmatrix} = \frac{\lambda^2}{4\pi^2r_1^2}\begin{pmatrix} |S_2|^2 \\ |S_1|^2 \end{pmatrix}, \quad (32)$$

where

$$S_2 = \sum_{n=1}^{\infty}\sum_{m=-n}^{+n}[c_{nm}m\tilde{\pi}_n^m(\cos\theta) - d_{nm}\tilde{\tau}_n^m(\cos\theta)]i^{n+1}(-1)^m\exp(im\varphi), \quad (33)$$

$$S_1 = \sum_{n=1}^{\infty}\sum_{m=-n}^{+n}[c_{nm}\tilde{\tau}_n^m(\cos\theta) - d_{nm}m\tilde{\pi}_n^m(\cos\theta)]i^{n+1}(-1)^m\exp(im\varphi). \quad (34)$$

3. NUMERICAL RESULTS

A computer program is written in FORTRAN relying on the theoretical work stated above. Thanks to the programs published and maintained on the Internet, such as the one from Wriedt [56], it allows almost instant verification of results without costly software development for some commonly used subroutines. For instance, the required Ricatti–Bessel functions in our program are evaluated using the recursion algorithm presented by Ngo *et al.* [35]. The most significant differences between our code and the one from Ngo *et al.* are as follows. (i) Plane wave illumination is generalized to arbitrary shaped beam illumination. Specifically, the BSCs, for Gaussian beam illumination, are determined using the Modified Localized Approximation method developed by Gouesbet *et al.* [6,16,17,54]. (ii) Subroutines for evaluations of internal and near-surface field distributions are developed.

Furthermore, for the aim of developing a more convergent computer program, the associated Legendre functions are evaluated in terms of Wigner d functions, which achieve good convergence even when the order is very large [57]. The translational coefficients of the VSWFs are evaluated according to the recurrence relationship provided by Mackowski [48] instead of the one proposed by Bobbert and Vlieger [47] and used by Ngo *et al.* [35]. Although several modifications have been made, the convergent problem reported in Ngo's code [58] also exists in our code. Nevertheless, it has little influence on the analysis of field intensity distributions in the present paper.

Regarding the numerical evaluation of the elements H_{sn}^m in Eq. (18), Han *et al.* [36] calculated them (although with a different notation and presentation) by using a summation of a finite number of terms that satisfy the following four conditions: (i) $\sigma \le 0$, (ii) $\sigma \le -(m+m')$, (iii) $\sigma \le n-m$, (iv) $\sigma \le n-m'$. This was a fairly tedious procedure so that, for this paper, we use a somewhat more efficient method. Let us recall Eq. (102) in [22]; we can rewrite Eq. (18) as

$$H_{sn}^m = \left[\frac{(n-m)!(n+s)!}{(n+m)!(n-s)!}\right]^{1/2}e^{im\gamma}e^{is\alpha}d_{ms}^n, \quad (35)$$

where d_{ms}^n is the Wigner d function, which can be evaluated by a recurrence relation [57], which is given in Appendix B for the sake of convenience.

A. Numerical Test Cases

As a verification of the homemade program as well as of the theoretical derivations for an arbitrary shaped beam in an arbitrary orientation, we have compared our results with those published by Ngo *et al.* [35] in the case of plane wave illumination. All the results concerning the extinction and scattering efficiencies coincide with each other at least in four digits.

As another verification of the code, comparisons between the results obtained from our code are compared with those published by Han *et al.* [36] and Yan *et al.* [37]. As we noticed, only results for special cases of on-axis Gaussian beam illumination were presented by Yan *et al.* [37]. We prefer to present a comparison of scattered intensity distribution for a general case of off-axis Gaussian beam illumination in Fig. 2 between the results obtained from our code and those published by Han *et al.* [36]. In this comparison, parameters are adopted directly from [36]. The radii of the inclusion and of the host sphere are $0.5\,\mu$m and $1.0\,\mu$m with complex refractive indices of $1.55 + 0.0i$ and $1.33 + 0.0i$, respectively. The center–center separation distance is $d = 0.25\,\mu$m. It is illuminated by a Gaussian beam at incidence angles $\alpha = \gamma = 0.0°$, $\beta = 45.0°$, with wavelength $\lambda = 0.6328\,\mu$m and beam waist $w_0 = 1.0\,\mu$m. The location of the beam waist center is a varied parameter. Satisfactory agreements are achieved, although there may be some differences (logarithmic scales are used), especially in the forward- and backward-scattering direction.

Further verification is made by comparing spatial distributions of normalized source function for the internal and near-surface fields with published results for a sphere illuminated by plane wave [59].

Figure 4(a) shows the normalized source function distribution of the near-surface and internal fields along the z axis for a homogeneous spherical glass bead (having a complex refractive index $m = 1.5 + 0.0i$ and size parameter 20) illuminated by an x-axis direction polarized plane wave propagating along the $+z$ axis direction. The amplitude of the incident electromagnetic wave electric field has been set to unity. Spatial coordinates are normalized relative to the sphere radius. Results from our code are identical to those provided by Barber and Hill [59]. Particular values for exact checks are evaluated at points −2.5, −1.0, 1.0, and 2.5. The values obtained from our code are 0.87081, 1.4987, 59.2146, and 3.2682, respectively.

B. Numerical Results

1. Scattered Field in the Far Zone

Scattered field distributions resulting from a focused laser beam incident on a particle system are dependent on the properties of the incident electromagnetic beam (beam waist radius, location of beam waist center, wavelength, and incident orientation) as well as on the properties of the scatterer (shape, diameter, complex refractive index, etc.).

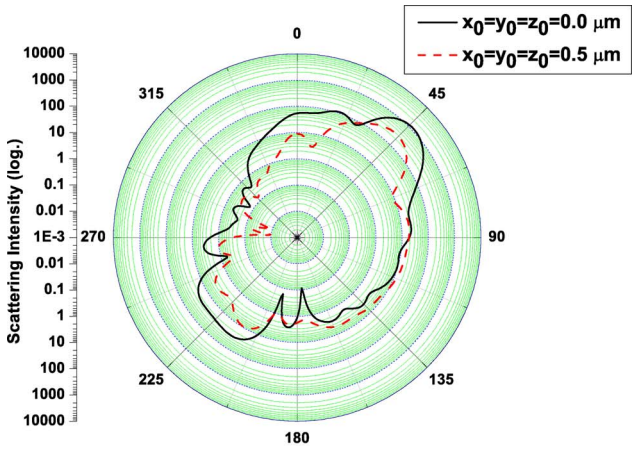

(a)

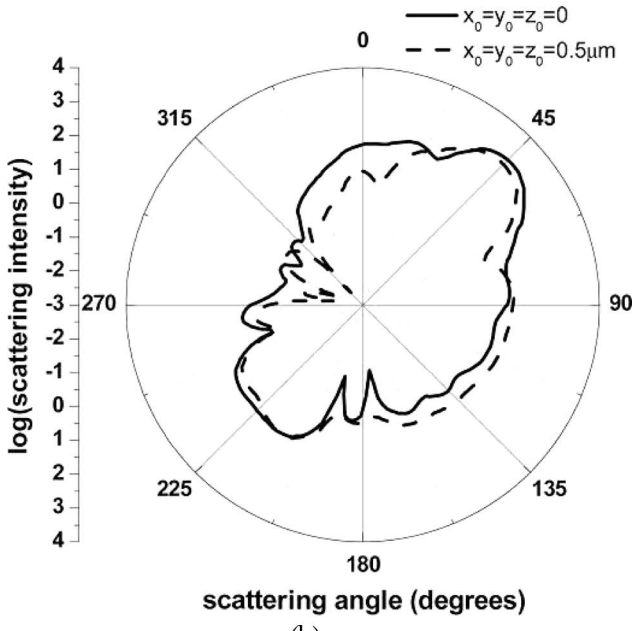

(b)

Fig. 2. (Color online) Comparison of scattered intensity distribution between the result obtained from our code and Fig. 6 published in [36].

Variations in spatial distributions of scattered field in the far zone from a spherical glass bead (having a complex refractive index $1.50 + 0.0i$) containing a spherical water inclusion (having a complex refractive index $1.33 + 0.0i$) are displayed in video format for different cases. The following parameters are applied except stated otherwise. The complex refractive index in the surrounding medium is set equal to unity. The radius of the host sphere is assumed to be $3.0\,\mu$m, and that of the inclusion is $1.50\,\mu$m. The incident electromagnetic focused Gaussian beam was assumed to be linearly polarized along the u axis at its waist with a wavelength equal to $0.6328\,\mu$m. Its beam waist center is located at the origin of the global coordinate system with $x_0 = y_0 = z_0 = 0.0\,\mu$m. The incident orientation is specified by Euler angles at $\alpha = \gamma = 0.0°$, $\beta = 90°$ so that the forward direction of the scattered field is at the center of the graphs ($\theta = 90°$, $\varphi = 0.0°$). Media 1 and Media 2 proceed along eight steps according to the scenario detailed below. The vertical axis in the movie is the zenith angle θ in degrees, and the horizontal axis is the azimuthal angle φ in degrees; scenery numbers are shown at the rightmost side to indicate the procedure of the movie. Single-frame pictures excerpted from Media 1 and Media 2 are shown in Fig. 3.

The movie begins with the inclusion situated at the center of the host sphere. The particle system is illuminated by a Gaussian beam with a pretty large beam waist, such as $w_0 = 50.0\,\mu$m; that is to say, plane wave illumination is applied. Then (i) the inclusion is translated along the z axis from the center of the host sphere $d = 0.0\,\mu$m to the edge at $d = 1.0\,\mu$m. Afterward, (ii) holding the position of the spherical inclusion constant at $d = 1.0\,\mu$m, we decrease the radius of the inclusion from $b = 1.5\,\mu$m to $b = 0.0\,\mu$m, which is followed by (iii) increasing the radius of the inclusion from $b = 0.0\,\mu$m to $b = 1.5\,\mu$m. The beam waist radius of the Gaussian beam is then (iv) decreased from $w_0 = 50.0\,\mu$m to $w_0 = 2.0\,\mu$m. That is to say, the plane wave illumination is replaced by a focused Gaussian beam illumination step-by-step, with a step of $5.0\,\mu$m in the range [$50.0\,\mu$m, $5.0\,\mu$m] and a step of $0.5\,\mu$m in the range [$5.0\,\mu$m, $2.0\,\mu$m]. Fixing the Gaussian beam waist at $w_0 = 2.0\,\mu$m and holding the position of the inclusion constant at $d = 1.0\,\mu$m, we (v) decrease the radius of the inclusion from $b = 1.5\,\mu$m to $b = 0.0\,\mu$m, which is followed by (vi) an increase from $b = 0.0\,\mu$m to $b = 1.5\,\mu$m. The inclusion then (vii) translates to the center of the host sphere with $d = 0.0\,\mu$m. At the end of the movie, (viii) we move the beam waist center of the focused Gaussian beam toward the edge of the host sphere along the z axis with $z_0 = 2.0\,\mu$m.

As we can notice from the movie, either in the illumination of a plane wave or in the illumination of a focused Gaussian beam, a second set of diffractionlike rings can be observed when the symmetry of the particle system is broken. The inclusion acts as a second radiating source, contributing to an interference structure in the scattering pattern, the spatial frequency of which varies with the location and the radius of the inclusion. A butterfly pattern is noticed growing up as the center–center separation distance increases. With a decrease in the inclusion radius, the wings of the butterfly seems to diffuse laterally (the inclusion becoming smaller, with a larger radius of curvature, throws rays away more efficiently in the lateral directions),

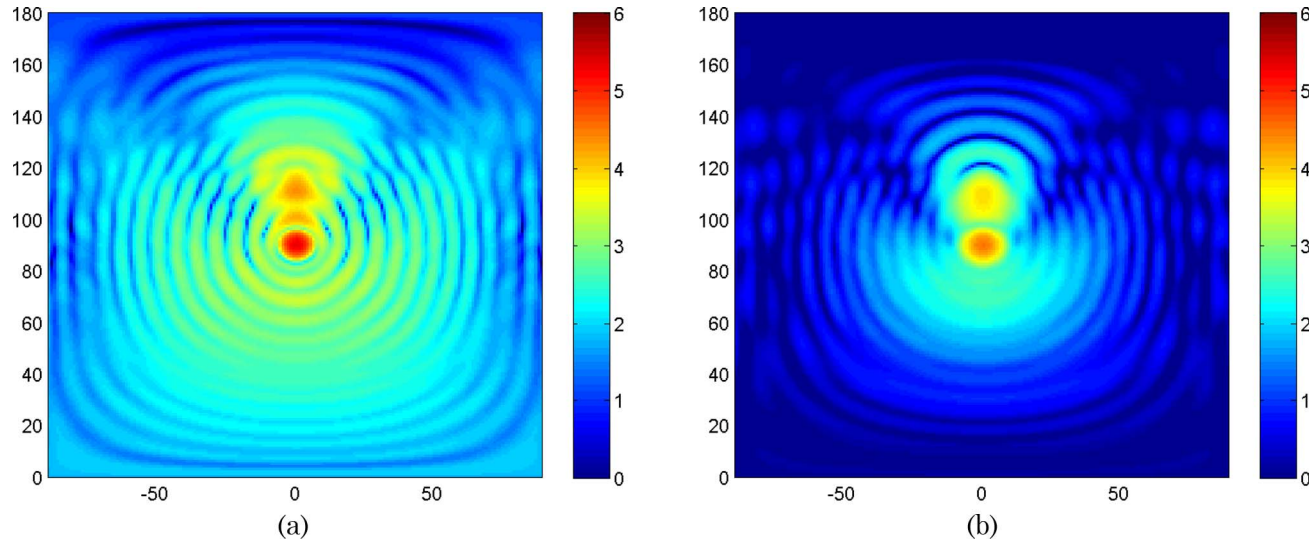

Fig. 3. (Color online) Scattered field distribution in the far zone. (a) Single-frame excerpt from Media 1 for cases of plane wave illumination. (b) Single-frame excerpt from Media 2 for cases of focused Gaussian beam illumination. The vertical axis in the movie is the zenith angle θ in degrees, and the horizontal axis is the azimuthal angle φ in degrees..

also become weaker since the inclusion is smaller, and at last disappear when the inclusion disappears.

During the procedure of plane wave illumination replaced step-by-step by Gaussian beam illumination, for most of the time we do not observe any significant variation in the scattering pattern, in accordance with the fact that the radius of the host sphere is $3.0\,\mu$m, which is much smaller than the beam waist radius, so that, for most of the time, the illumination is still essentially the one of a plane wave. When Gaussian beam effects become significant, we conversely observe a strong modification of the scattering pattern, in which an image of the inclusion in the scattering pattern becomes more and more apparent in the forward direction, while as a whole the interference pattern simplifies, with many rings progressively disappearing and much less light shed laterally.

At the last part of the movie, the inclusion is located at the center of the host sphere; such a geometry actually corresponds to the one of a coated sphere. We can observe a pattern with a maximal spherical symmetry (spherical symmetry of the scatterer, and location of the beam waist center at the center of the scatterer). When the beam waist center of the Gaussian beam is moved toward the edge of the host sphere, a progressive and eventually very significant loss of symmetry can be noticed, in which the original maximal spherical symmetry is broken. This evolution corresponds to the development of a similar butterfly pattern, but with wings stretching in the downward direction instead of in the upward directions as we saw in the first half of the movie.

2. Near-Surface Field and Internal Field

Calculations of the internal and near-surface fields of a transparent sphere could be found in the case of plane wave illumination [59] and also in the case of shaped beam illumination [8]. Large enhancement of the near-surface field located in the shadow side of the particle was found both in the on-resonance conditions and in the off-resonance conditions. In the case of shaped beam illumination, the distribution of the internal and near-surface field is strongly dependent on the location of the focal center of the laser beam, which differs significantly from the corresponding results when the exciting resource is a plane wave. Nevertheless, most efforts have been found to be devoted to spherical particles, but other shapes or composite particles are also of interest, such as a micrometer-sized particle containing a smaller eccentrically located inclusion under study in this paper. A series of calculations is then performed to demonstrate the effects of particle system geometry, orientation, and focal center location of the Gaussian beam on the spatial distributions of internal and near-surface fields.

Specifically, near-surface and internal fields distributions are calculated for a glass sphere (having a real refractive index equal to 1.50) with an eccentrically located water droplet (having a real refractive index equal to 1.33) in the case of plane wave illumination and in the case of a focused Gaussian beam illumination. The incident beam (plane wave or Gaussian beam) is originally assumed to propagate in the $+z$-axis direction with electric field vector polarized along the x axis (at the waist) with wavelength $0.6283\,\mu$m. The beam waist radius of the Gaussian beam is assumed to be $\omega_0 = 1.6\,\mu$m, which is smaller than the radius of the host sphere $a = 2.0\,\mu$m, while greater than the radius of the inclusion $b = 1.0\,\mu$m.

As aforementioned, even though the magnitude and the phase for each component of the electromagnetic field can be determined, a useful visualization of the electromagnetic field distribution can be obtained by plotting the normalized source function as a function of spatial position. Normalized source functions are calculated on a normalized square grid of dimension $2r/a \times 2r/a$. Two hundred points along the z axis and 100 points along the x axis are used in Figs. 4 and 5, due to the fact that, in these cases, the intensity variation along the x axis is much slower than that along the z axis. Nevertheless, 200 points are used both along the z axis and along the x axis in Figs. 7 and 8, which are the cases when the shaped beam is incident on the particle obliquely. It is worth mentioning that if too many points are used in the calculation of internal field distribution, the calculation of the Bessel functions may become unstable for radii near the origin, since the argument of the functions will be much smaller than the order.

Normalized source function distributions along the z axis are displayed in Fig. 4, and distributions over the equatorial

plane (x–z plane) are shown in Fig. 5 as a function of the center–center separation distance d.

In Fig. 4(a), the well-known high intensity peak in the near-surface field behind the scatterer dominates the graph, whose intensity is more than 100 times the incident beam intensity. Nevertheless, this large broad intensity peak is afterward significantly spoiled due to the existence of an inclusion, as observed in Figs. 4(b) and 4(c). Furthermore, when the plane wave illumination is replaced by a focused Gaussian beam illumination in Figs. 4(d)–4(f), the high intensity peak is also reduced greatly. In a further study (results are not shown here), we find that the narrower the Gaussian beam waist is, the lower the intensity of the high energy peak will be. Thus, we may come to the conclusion that the focusing effect caused by the curved surface of host spherical particle plays a main role in the construction of the high intensity peak in the shadow side of the host sphere, which is similar to the transmission spherical aberration caustic in the optical system. This conclusion is also supported by the fact that several intensity peaks are observed in the shadow side of the inclusion, which may mainly be due to the focusing effect of the spherical inclusion.

The other prominent feature in Fig. 4 is that a small intensity peak observed in the illuminated side of the host sphere

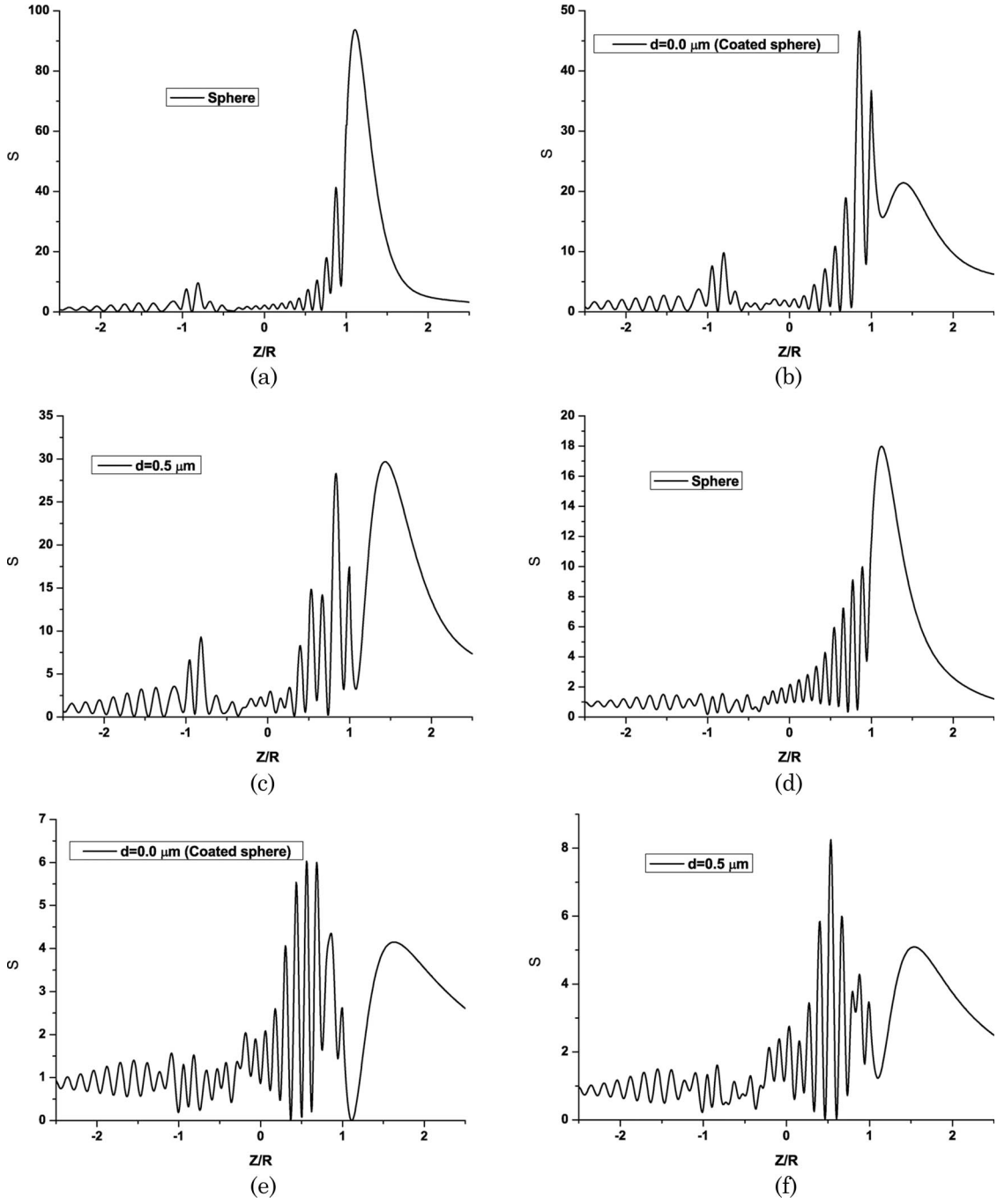

Fig. 4. Normalized source function for external and internal fields along the z axis with center–center separation distance d as the parameter. The left column [(a), (b), (c)] is for cases of plane wave illumination; the right column [(d), (e), (f)] is for cases of focused Gaussian beam illumination.

(the small peak located at approximately $z/R = -0.8$) in the case of plane wave illumination is significantly degenerated when a focused Gaussian beam illumination is applied. From a point of view of ray theory, this peak is claimed to be constructed by the crossing of the arms of the interior focusing caustic for three internal reflections [60]. And the numerical results obtained here emphasize that the construction of this peak is crucially associated with the off-axis partial waves propagating in the A zone depicted in Fig. 6.

The features found in Fig. 4 can also be observed in Fig. 5. Furthermore, if we look closely into the interior of the host sphere, three energy flows toward the shadow side of the host sphere can be apparently observed when the host sphere is illuminated by a plane wave. The main energy flows in the middle is greatly enhanced in the case of focused beam illumination, while the other two energy flows in the lateral sides are blurred or even disappear.

Spatial distributions of normalized source functions over the equatorial plane (x–z plane) are shown in Fig. 7 as a function of the incident direction of the Gaussian beam. The spherical inclusion is located on the z axis with center–center separation distance $d = 0.5$. A focused Gaussian beam illuminates the particle system with Euler angles $\alpha = \gamma = 0.0°$ and β as a parameter. The beam waist center of the Gaussian beam locates at the center of the host sphere with $x_0 = y_0 = z_0 = 0.0$.

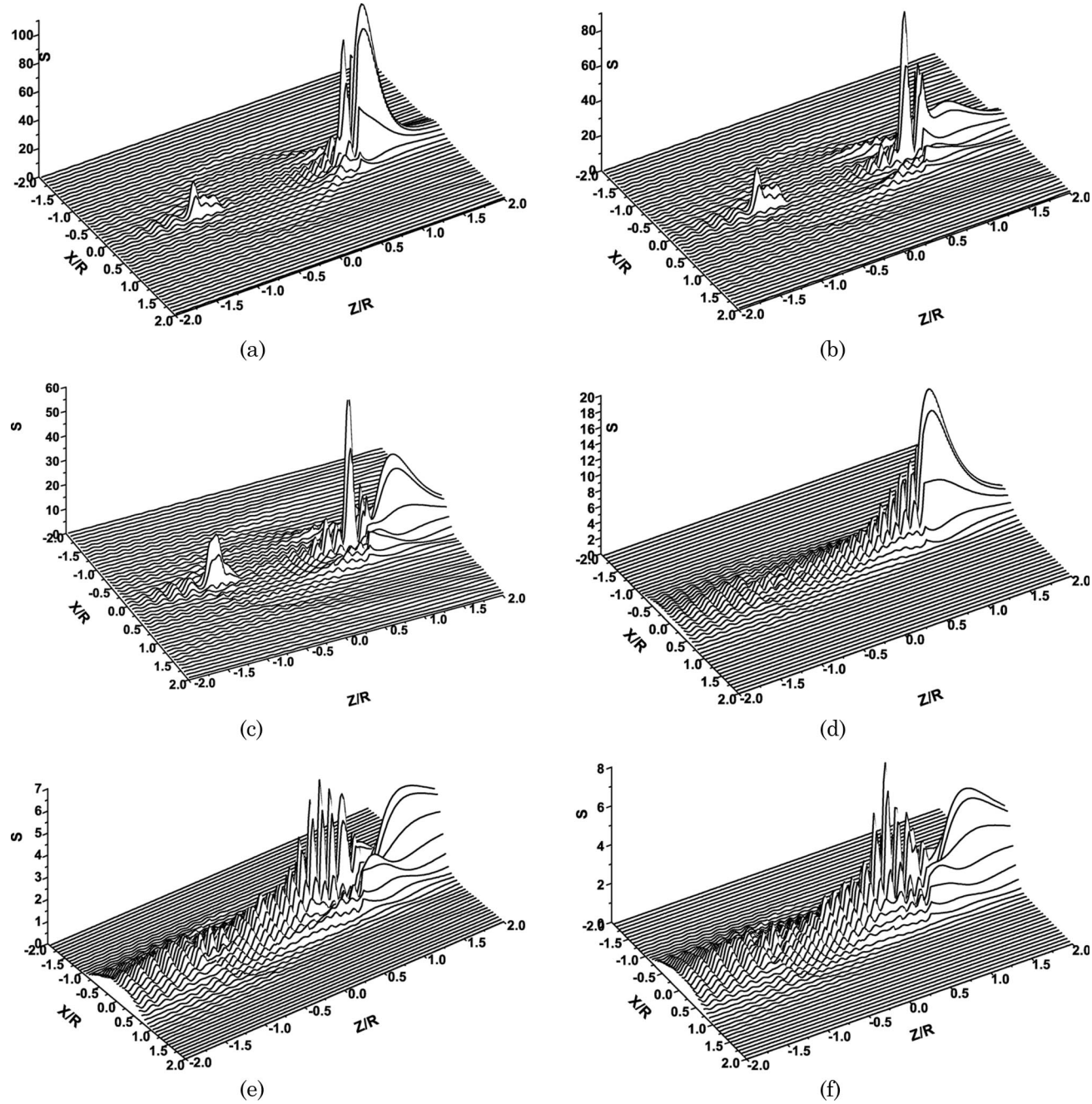

Fig. 5. Normalized source function for external and internal field over the x–z plane with center–center separation distance d as the parameter. The left column [(a), (b), (c)] is for cases of plane wave illumination; the right column [(d), (e), (f)] is for cases of focused Gaussian beam illumination.

Comparing Fig. 7(a) with Figs. 7(b)–7(d), we can observe that, when the particle system with a broken spherical symmetry is illuminated obliquely by a focused Gaussian beam, the scattered field resulting from scattering of the inclusion interferes with the incident beam, which is refracted once by the host sphere surface, to create a complex interference pattern in the internal field. This interference pattern contributes to the features that the main electromagnetic energy propagates along a different track from that of the incident beam direction; a branch of electromagnetic energy is observed to be divided from the main energy flows.

Spatial distributions of normalized source functions over the equatorial plane (x–z plane) are shown in Fig. 8, as a function of location of the Gaussian beam waist center. The spherical inclusion is located on the z axis with center–center separation distance $d = 0.5$. A focused Gaussian beam illuminates the particle system with Euler angles $\alpha = \gamma = 0.0°$ and $\beta = 90°$; that is to say, it propagates along the x axis from left to right in the figures. The position of the beam waist center of the Gaussian beam is assumed to be $x_0 = y_0 = 0.0$ and z_0 as a parameter.

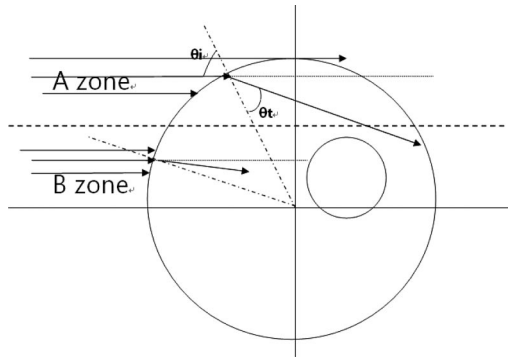

Fig. 6. Illustration of localization of partial waves in a geometric optics point of view.

Figure 8 shows the behavior of an off-axis Gaussian beam when it transmits through a host sphere with an eccentrically

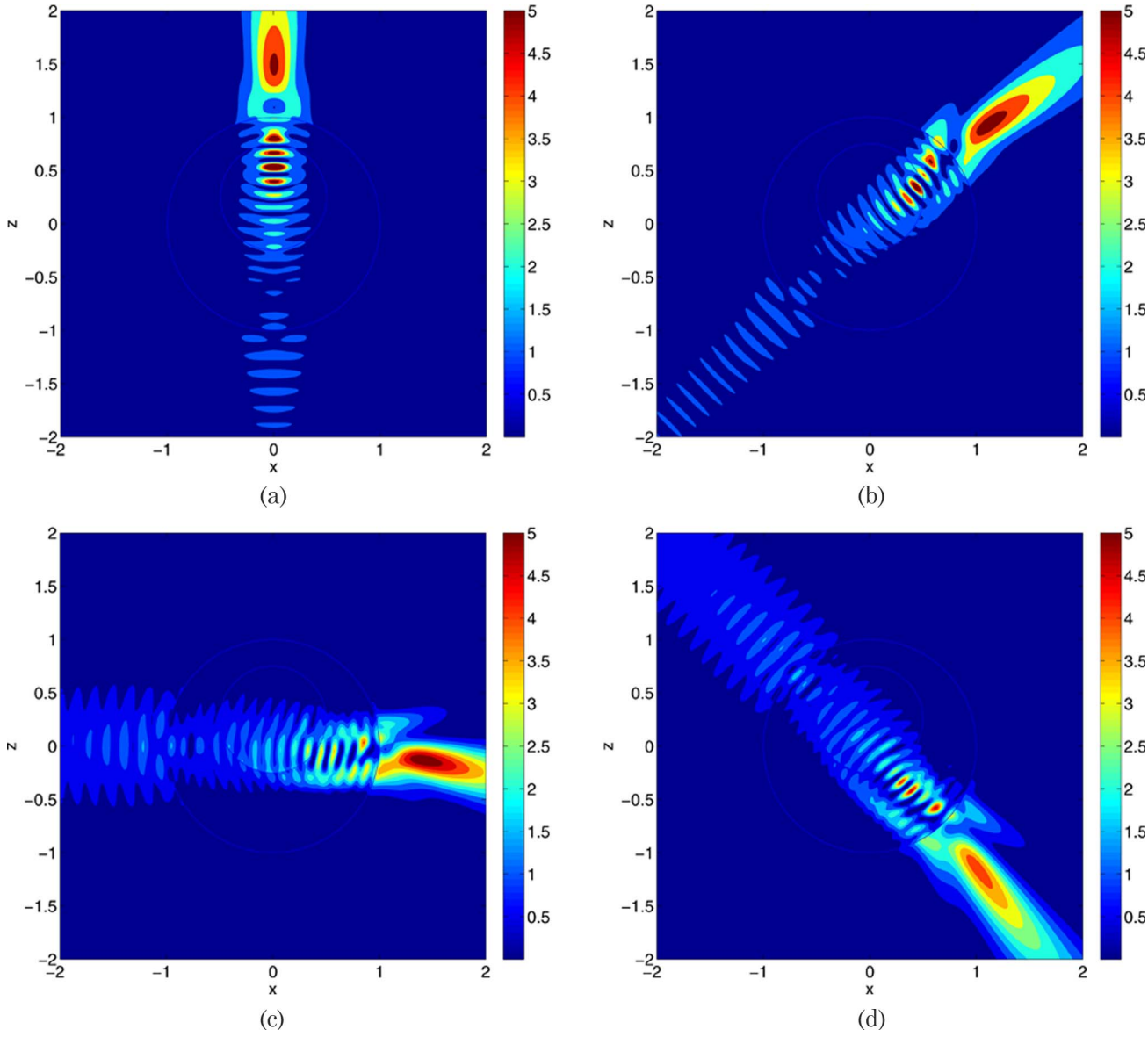

Fig. 7. (Color online) Normalized source function distribution for external and internal fields over the x–z plane with Euler angles $\alpha = \gamma = 0.0°$ and β as a parameter..

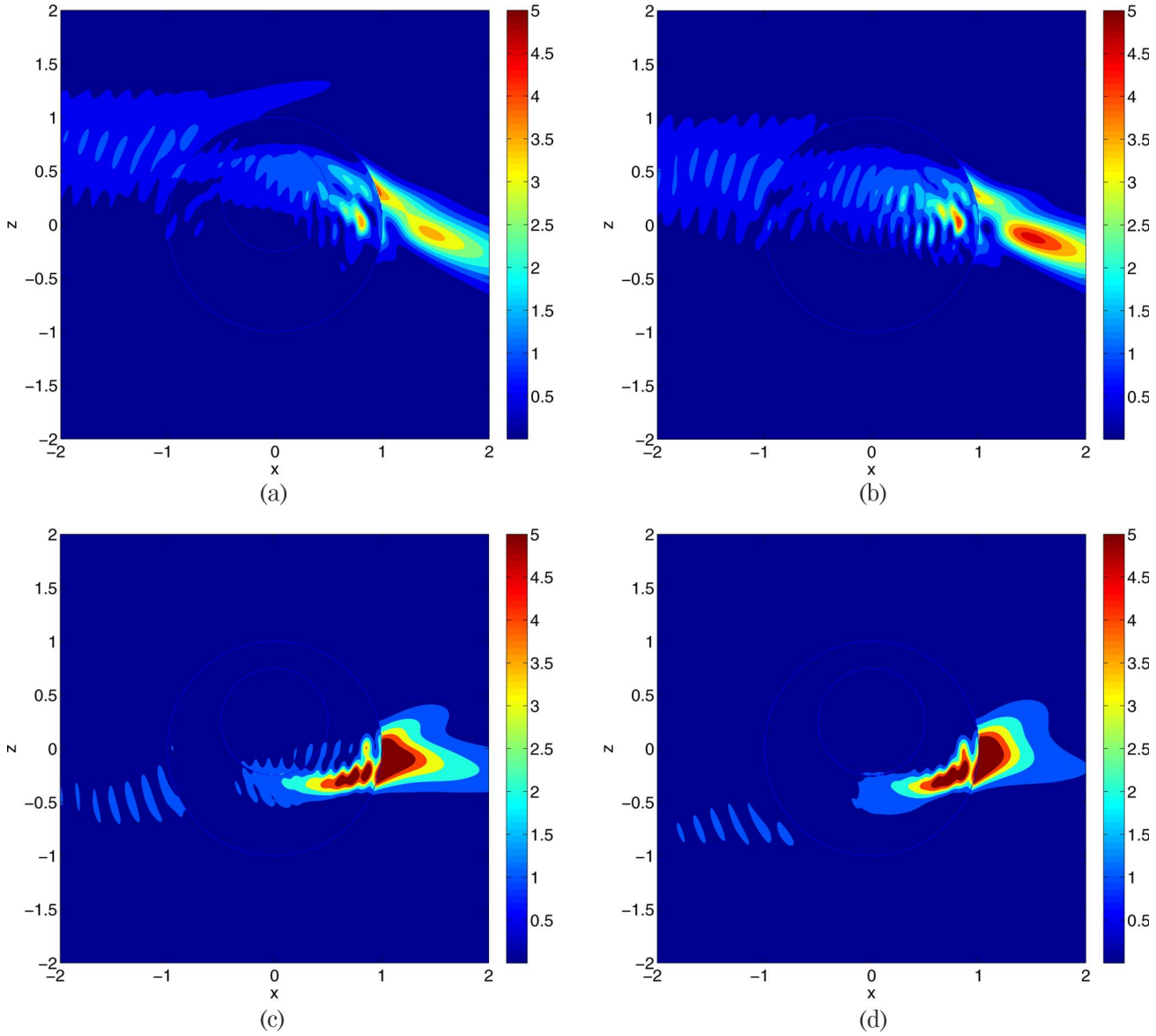

Fig. 8. (Color online) Normalized source function distribution for external and internal field over the x–z plane with location of the Gaussian beam waist center as a parameter. The Gaussian beam propagates along the x axis from left to right..

located spherical inclusion. Generally speaking, when the beam waist center of the Gaussian beam is not located at the center of the host sphere, that is to say, more partial waves with higher electromagnetic energy density become off-axis, the propagation direction of the Gaussian beam is bent toward the horizontal center-line (the x axis) due to the refraction effect at the surface of the host sphere. The farther the beam waist center is away from the host sphere center, the larger the incident angle is, which leads to a larger turning angle between the propagation direction after refraction and the original propagation direction. In the meanwhile, more energy is reflected back into the surrounding medium with the increase of the incident angle; a clear nonsymmetric interference pattern can be observed in the backward-scattering direction. These features are very similar to the case of a bunch of rays strikes on a sphere of large size parameter as shown in Fig. 6. Nevertheless, the scattering behavior becomes more complicated in the problem under study, especially the field distributions inside the particle, which is very sensitive to the relative location of the inclusion inside the host sphere.

4. CONCLUSION

Based on the recent improvements in the GLMT concerning the evaluation of BSCs [20–24], this paper presents a study on the scattering problem of a sphere with an eccentrically located spherical inclusion illuminated by an arbitrary shaped electromagnetic beam in an arbitrary orientation. A computer program is written in FORTRAN based on the theoretical work, which permits the prediction of various scattering data. Besides completing the scattering results in the far zone published in [36,37], numerical results concerning spatial distributions of the near-surface field outside of the host sphere and internal field inside the host sphere are presented for the first time in this paper for various parameter values, such as regarding orientation of the incident Gaussian beam, location of the beam waist center of the Gaussian beam, and location of the spherical inclusion.

Concerning the scattered field distributions in the far zone, when the symmetry of the problem is broken (either due to a loss of symmetry of the particle configuration or to a loss of symmetry of the location of the illuminating beam), the symmetry of the scattering pattern in the far zone is broken as well. The inclusion acts as a second radiating source, contributing to an interference structure in the scattering pattern. A second set of diffractionlike rings is observed with lower intensity relative to the main diffraction rings, whose frequency varies significantly depending on the location and radius of the inclusion. Well-apparent butterfly patterns can be observed in the movies, associated with symmetry breakings. Such symmetry breakings arise when the inclusion is more and more eccentrically located, instead of being located at the center of the host sphere (coated sphere problem), or when the beam waist center of the Gaussian beam is not situated at the center of the host sphere. Focused Gaussian beam effects have also been underlined in which radiating sources (host sphere and inclusion) appear to be more focused and brighter, with an enhancement and spreading of the interference structure, with respect to plane wave illumination.

From numerical results concerning spatial distributions of near-surface and internal fields, we can notice that the well-known high intensity peak in the near-surface field behind the scatterer, whose intensity could be more than 100 times the incident plane wave intensity, is degenerated significantly due to the existence of an inclusion or when the plane wave illumination is replaced by a focused Gaussian beam illumination. Furthermore, the narrower the Gaussian beam waist is, the lower the intensity of the high energy peak will be, indicating that the focusing effect caused by the curved surface of host spherical particle plays a significant role in the construction of the high intensity peak in the shadow side of the host sphere, which is similar to the transmission spherical aberration caustic in optical systems.

Another prominent feature is that the peak observed in the illuminated side of the host sphere in the case of plane wave illumination is significantly degenerated when a focused Gaussian beam illumination is applied, which indicates that the construction of this peak is greatly associated with the off-axis partial waves propagating in the A zone depicted in Fig. 6.

When the particle system with broken spherical symmetry is illuminated obliquely by a focused Gaussian beam, the main energy flows are observed to be out of the original track along the propagation direction of the incident beam. A branch of energy is divided from the main energy flows. Furthermore, when the beam waist center of the Gaussian beam is not located in the center of the host sphere, the incident beam is bent toward the horizontal centerline along the x axis due to the refraction effect at the surface of the host sphere. The farther the beam waist center is away from the host sphere center, the larger the turning angle between the refraction direction and the original propagation direction would be. In the meanwhile, a larger fraction of electromagnetic energy is reflected back into the surrounding medium with the increase of the incident angle; a clear nonsymmetric interference pattern can be observed in the backward scattering direction.

The original motivation of our present work lies on the future detection of the interesting optical (Hamiltonian) chaos features depicted in [39–41], which are raised by the complex optical interactions between the eccentrically located inclusion with the host sphere, in the case of loss of spherical symmetry. The study on internal and near-surface field distribution would contribute to the understanding of multiple scattering interactions between closely spaced particles or between different parts of a scattering system, such as the scattering model under study. It would also have contributions to the study of the nonlinear optical mechanisms leading to lasering in cavity quantum electrodynamic (QED) as well as to the improvement of optical sensors and imaging, such as the study of fluorescence and Raman effects. Furthermore, the work on scattered field distributions would be helpful to the improvements of relevant laser-related detecting techniques, such as in the field of particle characterization or identification of internal nonuniformities.

APPENDIX A

In general, the translational addition theorem for VSWFs can be written

$$\mathbf{M}_{nm}^{(i)}(k\mathbf{r}) = \sum_{n'=1}^{\infty}\sum_{m=-n'}^{n'} A_{m'n'}^{mn}(k\mathbf{r_0})\mathbf{M}_{n'm'}^{(i)}(k\mathbf{r_1}) + B_{m'n'}^{mn}(k\mathbf{r_0})\mathbf{N}_{n'm'}^{(i)}(k\mathbf{r_1}), \tag{A1}$$

$$\mathbf{N}_{nm}^{(i)}(k\mathbf{r}) = \sum_{n'=1}^{\infty}\sum_{m=-n'}^{n'} B_{m'n'}^{mn}(k\mathbf{r_0})\mathbf{M}_{n'm'}^{(i)}(k\mathbf{r_1}) + A_{m'n'}^{mn}(k\mathbf{r_0})\mathbf{N}_{n'm'}^{(i)}(k\mathbf{r_1}). \tag{A2}$$

If the translation is along the z axis, the double summation above reduces to a single summation over the index n'. So we obtain

$$\mathbf{M}_{nm}^{(i)}(k\mathbf{r}) = \sum_{n'=1}^{\infty} A_{nn'}^{m}(k\mathbf{r_0})\mathbf{M}_{n'm}^{(i)}(k\mathbf{r_1}) + B_{nn'}^{m}(k\mathbf{r_0})\mathbf{N}_{n'm}^{(i)}(k\mathbf{r_1}), \tag{A3}$$

$$\mathbf{N}_{nm}^{(i)}(k\mathbf{r}) = \sum_{n'=1}^{\infty} B_{nn'}^{m}(k\mathbf{r_0})\mathbf{M}_{n'm}^{(i)}(k\mathbf{r_1}) + A_{nn'}^{m}(k\mathbf{r_0})\mathbf{N}_{n'm}^{(i)}(k\mathbf{r_1}). \tag{A4}$$

For axial translations and positive values of m, the vector addition coefficients $A_{mn'}^{mn}$ and $B_{mn'}^{mn}$ can be related to the scalar addition coefficients $C_{mn'}^{mn}$:

$$A_{mn'}^{mn}(k\mathbf{z_0}) = C_{mn'}^{mn}(k\mathbf{z_0}) + \frac{kz_0}{n'+1}\sqrt{\frac{(n'-m+1)(n'+m+1)}{(2n'+1)(2n'+3)}}C_{mn'+1}^{mn}(k\mathbf{z_0}) + \frac{kz_0}{n'}\sqrt{\frac{(n'-m)(n'+m)}{(2n'+1)(2n'-1)}}C_{mn'-1}^{mn}(k\mathbf{z_0}), \tag{A5}$$

$$B_{mn'}^{mn}(k\mathbf{z_0}) = jkz_0\frac{m}{n'(n'+1)}C_{mn'}^{mn}(k\mathbf{z_0}). \tag{A6}$$

For negative values of the index m, the following symmetry relations can be used for practical calculations:

$$A^{-mn}_{-mn'}(k\mathbf{z_0}) = A^{mn}_{mn'}(k\mathbf{z_0}), \qquad B^{-mn}_{-mn'}(k\mathbf{z_0}) = -B^{mn}_{mn'}(k\mathbf{z_0}), \quad \text{(A7)}$$

$$A^{-mn}_{-mn'}(k\mathbf{z_0}) = A^{mn}_{mn'}(-k\mathbf{z_0}), \qquad B^{-mn}_{-mn'}(k\mathbf{z_0}) = B^{mn}_{mn'}(-k\mathbf{z_0}). \quad \text{(A8)}$$

The recurrence relations for the $C^{mn}_{mn'}$ coefficients are simple in the case of axial translation and positive m:

$$\begin{aligned}
&\sqrt{\frac{(n-m+1)(n+m+1)}{(2n+1)(2n+3)}}C^{mn+1}_{mn'}(k\mathbf{z_0}) \\
&- \sqrt{\frac{(n-m)(n+m)}{(2n-1)(2n+1)}}C^{mn-1}_{mn'}(k\mathbf{z_0}) \\
&= \sqrt{\frac{(n'-m)(n'+m)}{(2n'-1)(2n'+1)}}C^{mn}_{mn'-1}(k\mathbf{z_0}) \\
&\quad - \sqrt{\frac{(n'-m+1)(n'+m+1)}{(2n'+1)(2n'+3)}}C^{mn}_{mn'+1}(k\mathbf{z_0}),
\end{aligned} \quad \text{(A9)}$$

$$\begin{aligned}
&\sqrt{\frac{(n-m-1)(n-m+1)}{(2n-1)(2n+1)}}C^{mn-1}_{mn'}(k\mathbf{z_0}) \\
&+ \sqrt{\frac{(n+m)(n+m+1)}{(2n+1)(2n+3)}}C^{mn+1}_{mn'}(k\mathbf{z_0}) \\
&= \sqrt{\frac{(n'+m-1)(n'+m)}{(2n'-1)(2n'+1)}}C^{m-1n}_{m-1n'-1}(k\mathbf{z_0}) \\
&\quad + \sqrt{\frac{(n'-m+1)(n'-m+2)}{(2n'+1)(2n'+3)}}C^{m-1n}_{m-1n'+1}(k\mathbf{z_0}).
\end{aligned} \quad \text{(A10)}$$

The convention $C^{mn}_{mn'} = 0$ for $m > n$ and $m > n'$ is assumed in the above equations.

Initial values are given:

$$\begin{aligned}
&C^{00,(1)}_{0n'}(k\mathbf{z_0}) = (-1)^{n'}\sqrt{2n'+1}j_{n'}(k\mathbf{z_0}) \\
&\text{for regular VSWFs translation,} \\
&C^{00,(3)}_{0n'}(k\mathbf{z_0}) = (-1)^{n'}\sqrt{2n'+1}h^{(1)}_{n'}(k\mathbf{z_0}) \\
&\text{for radiating VSWFs translation.}
\end{aligned} \quad \text{(A11)}$$

APPENDIX B

The recurrence relation for the Wigner d functions are given below, which can also be found in [57], Appendix B:

$$\begin{aligned}
d^{n+1}_{ms}(\beta) = &\frac{1}{n\sqrt{(n+1)^2-m^2}\sqrt{(n+1)^2-s^2}}\{(2n \\
&+1)[n(n+1)x - ms]d^n_{ms}(\beta) \\
&-(n+1)\sqrt{n^2-m^2}\sqrt{n^2-s^2}d^{n-1}_{ms}(\beta)\},
\end{aligned} \quad \text{(B1)}$$

$n \geq n_{\min}$.

Initial values are given:

$$d^{n_{\min}-1}_{ms}(\beta) = 0, \quad \text{(B2)}$$

$$\begin{aligned}
d^{n_{\min}}_{ms}(\beta) = &\xi_{ms}2^{-n_{\min}}\left[\frac{(2n_{\min})!}{(|m-s|)!|m+s|!}\right]^{1/2} \\
&\times (1-x)^{|m-s|/2}(1+x)^{|m+s|/2},
\end{aligned} \quad \text{(B3)}$$

in which

$$\xi_{ms} = \begin{cases} 1 & \text{if } s \geq m \\ (-1)^{m-s} & \text{if } s < m \end{cases}, \quad \text{(B4)}$$

$$n_{\min} = \max(|m|,|s|), \qquad x = \cos\beta. \quad \text{(B5)}$$

The Wigner d functions have real values and share the following symmetry properties:

$$d^n_{ms}(\beta) = (-1)^{m+s}d^n_{-m,-s}(\beta) = d^n_{-s,-m}(\beta), \quad \text{(B6)}$$

$$d^n_{ms}(\pi-\beta) = (-1)^{n-s}d^n_{-ms}(\beta) = (-1)^{n-m}d^n_{m,-s}(\beta). \quad \text{(B7)}$$

By specifying $s = 0$, we can obtain the associated Legendre functions in terms of the Wigner d functions:

$$d^n_{m0}(\beta) = \sqrt{\frac{(n-m)!}{(n+m)!}}P^m_n(\cos\beta), \quad \text{(B8)}$$

in which $P^m_n(\cos\beta)$ are the associated Legendre functions. With some straightforward derivations, we can obtain

$$m\tilde{\pi}^m_n(\cos\beta) = -(-1)^m\sqrt{\frac{2n+1}{2}}\frac{\sqrt{n(n+1)}}{2}[d^n_{m1}(\beta) + d^n_{m-1}(\beta)], \quad \text{(B9)}$$

$$\tilde{\tau}^m_n(\cos\beta) = -(-1)^m\sqrt{\frac{2n+1}{2}}\frac{\sqrt{n(n+1)}}{2}[d^n_{m1}(\beta) - d^n_{m-1}(\beta)], \quad \text{(B10)}$$

$$\tilde{P}^m_n(\cos\beta) = (-1)^m\sqrt{\frac{2n+1}{2}}d^n_{m0}(\beta). \quad \text{(B11)}$$

ACKNOWLEDGMENTS

The work presented in this paper is supported by the project "Bourses Doctorales en Alternance" between France and China. This work is also partially supported by the National Natural Science Foundation of China (NSFC) (grant 60771039) and by the European program INTERREG

IVa-C5: Cross-Channel Centre for Low Carbon Combustion. The authors thanks especially the two reviewers for providing several constructive comments and suggestions to the present paper.

REFERENCES

1. G. Mie, "Beiträge zur optik trüben medien speziell kolloidaler metalösungen," Ann. Phys. **25**, 377–452 (1908).
2. J. A. Lock and G. Gouesbet, "Generalized Lorenz–Mie theory and applications," J. Quant. Spectrosc. Radiat. Transfer **110**, 800–807 (2009).
3. G. Gouesbet, "Generalized Lorenz–Mie theories, the third decade: a perspective," J. Quant. Spectrosc. Radiat. Transfer **110**, 1223–1238 (2009).
4. G. Gouesbet, B. Maheu, and G. Gréhan, "Light scattering from a sphere arbitrarily located in a Gaussian beam, using a Bromwich formulation," J. Opt. Soc. Am. A **5**, 1427–1443 (1988).
5. B. Maheu, G. Gouesbet, and G. Gréhan, "A concise presentation of the generalized Lorenz–Mie theory for arbitrary location of the scatter in an arbitrary incident profile," J. Opt. **19**, 59–67 (1988).
6. G. Gouesbet, "Validity of the localized approximation for arbitrary shaped beams in the generalized Lorenz–Mie theory for spheres," J. Opt. Soc. Am. A **16**, 1641–1650 (1999).
7. L. Méès, G. Gouesbet, and G. Gréhan, "Transient internal and scattered fields from a multi-layered sphere illuminated by a pulsed laser," Opt. Commun. **282**, 4189–4193 (2009).
8. J. P. Barton, D. R. Alexander, and S. A. Schaub, "Internal and near-surface electromagnetic fields for a spherical particle irradiated by a focused laser beam," J. Appl. Phys. **64**, 1632–1639 (1988).
9. G. Gouesbet, "Interaction between an infinite cylinder and an arbitrary-shaped beam," Appl. Opt. **36**, 4292–4304 (1997).
10. G. Gouesbet and G. Gréhan, "Generalized Lorenz–Mie theory for a sphere with an eccentrically located spherical inclusion," J. Mod. Opt. **47**, 821–837 (2000).
11. Y. P. Han, G. Gréhan, and G. Gouesbet, "Generalized Lorenz–Mie theory for a spheroidal particle with off-axis Gaussian-beam illumination," Appl. Opt. **42**, 6621–6629 (2003).
12. F. Xu, K. F. Ren, G. Gouesbet, G. Gréhan, and X. Cai, "Generalized Lorenz–Mie theory for an arbitrary oriented, located, and shaped beam scattered by homogeneous spheroid," J. Opt. Soc. Am. A **24**, 119–131 (2007).
13. K. F. Ren, G. Gréhan, and G. Gouesbet, "Scattering of a Gaussian beam by an infinite cylinder in the framework of generalized Lorenz–Mie theory: formulation and numerical results," J. Opt. Soc. Am. A **14**, 3014–3025 (1997).
14. L. Méès, K. F. Ren, G. Gréhan, and G. Gouesbet, "Scattering of a Gaussian beam by an infinite cylinder with arbitrary location and arbitrary orientation: numerical results," Appl. Opt. **38**, 1867–1876 (1999).
15. G. Gouesbet and L. Méès, "Generalized Lorenz–Mie theory for infinitely long elliptical cylinders," J. Opt. Soc. Am. A **16**, 1333–1341 (1999).
16. J. A. Lock and G. Gouesbet, "Rigorous justification of the localized approximation to the beam-shape coefficients in generalized Lorenz–Mie theory. I. On-axis beams," J. Opt. Soc. Am. A **11**, 2503–2515 (1994).
17. G. Gouesbet and J. A. Lock, "Rigorous justification of the localized approximation to the beam-shape coefficients in generalized Lorenz–Mie theory. II. Off-axis beams," J. Opt. Soc. Am. A **11**, 2516–2525 (1994).
18. Y. P. Han, H. Y. Zhang, and G. X. Han, "The expansion coefficients of arbitrary shaped beam in oblique illumination," Opt. Express **15**, 735–746 (2007).
19. Y. P. Han, Y. Zhang, H. Y. Zhang, and G. X. Han, "Scattering of typical particles by beam shape in oblique illumination," J. Quant. Spectrosc. Radiat. Transfer **110**, 1375–1381 (2009).
20. G. Gouesbet, J. J. Wang, and Y. P. Han, "Transformations of spherical beam shape coefficients in generalized Lorenz–Mie theories through rotations of coordinate systems. I. General formulation," Opt. Commun. **283**, 3218–3225 (2010).
21. J. J. Wang, G. Gouesbet, and Y. P. Han, "Transformations of spherical beam shape coefficients in generalized Lorenz–Mie theories through rotations of coordinate systems. II. Axisymmetric beams," Opt. Commun. **283**, 3226–3234 (2010).
22. G. Gouesbet, J. J. Wang, and Y. P. Han, "Transformations of spherical beam shape coefficients in generalized Lorenz–Mie theories through rotations of coordinate systems. III. Special Euler angles," Opt. Commun. **283**, 3235–3243 (2010).
23. G. Gouesbet, J. J. Wang, Y. P. Han, and G. Gréhan, "Transformations of spherical beam shape coefficients in generalized Lorenz–Mie theories through rotations of coordinate systems. IV. Plane waves," Opt. Commun. **283**, 3244–3254 (2010).
24. G. Gouesbet, J. A. Lock, J. J. Wang, and G. Gréhan, "Transformations of spherical beam shape coefficients in generalized Lorenz–Mie theories through rotations of coordinate systems. V. Localized beam models," Opt. Commun. (to be published).
25. J. G. Fikioris and N. K. Uzunoglu, "Scattering from an eccentrically stratified dielectric sphere," J. Opt. Soc. Am. A **69**, 1359–1366 (1979).
26. F. Borghese, P. Denti, R. Saija, and O. I. Sindoni, "Optical properties of spheres containing several spherical inclusions," Appl. Opt. **33**, 484–493 (1994).
27. K. A. Fuller, "Morphology-dependent resonances in eccentrically stratified sphere," Opt. Lett. **19**, 1272–1274 (1994).
28. G. Videen, D. Ngo, P. Chylek, and R. G. Pinnick, "Light scattering from a sphere with an irregular inclusion," J. Opt. Soc. Am. A **12**, 922–928 (1995).
29. A. Doicu, T. Wriedt, and Y. A. Eremin, *Light Scattering by Systems of Particles: Null-Field Method with Discrete Sources: Theory and Programs* (Springer, 2006).
30. S. M. Hasheminejad and Y. Mirzaei, "Exact 3D elasticity solution for free vibrations of eccentric hollow sphere," J. Sound Vib. (to be published).
31. D. R. Secker, P. H. Kaye, R. S. Greenaway, E. Hirst, D. L. Bartley, and G. Videen, "Light scattering from deformed droplets and droplets with inclusions. I. Experimental results," Appl. Opt. **39**, 5023–5030 (2000).
32. G. Videen, W. Sun, Q. Fu, D. R. Secker, R. S. Greenaway, P. H. Kaye, E. Hirst, and D. Bartley, "Light scattering from deformed droplets and droplets with inclusions. II. Theoretical treatment," Appl. Opt. **39**, 5031–5039 (2000).
33. N. Riefler, R. Schuh, and T. Wriedt, "Investigation of a measurement technique to estimate concentration and size of inclusions in droplets," Meas. Sci. Technol. **18**, 2209–2218 (2007).
34. A. A. Riziq, M. Trainic, C. Erlick, E. Segre, and Y. Rudich, "Extinction efficiencies of coated absorbing aerosols measured by cavity ring down aerosol spectrometry," Atmos. Chem. Phys. **8**, 1823–1833 (2008).
35. D. Ngo, G. Videen, and P. Chýlek, "A FORTRAN code for the scattering of EM waves by a sphere with a nonconcentric spherical inclusion," Comput. Phys. Commun. **99**, 94–112 (1996).
36. G. X. Han, Y. P. Han, J. Y. Liu, and Y. Zhang, "Scattering of an eccentric sphere arbitrarily located in a shaped beam," J. Opt. Soc. Am. B **25**, 2064–2072 (2008).
37. B. Yan, X. Han, and K. F. Ren, "Scattering of a shaped beam by a spherical particle with an eccentric spherical inclusion," J. Opt. A Pure Appl. Opt. **11**, 015705 (2009).
38. S. Saengkaew, G. Godard, J. B. Blaisot, and G. Gréhan, "Experimental analysis of global rainbow technique: sensitivity of temperature and size distribution measurements to non-spherical droplets," Exp. Fluids **47**, 839–848 (2009).
39. G. Gouesbet, S. Meunier-Guttin-Cluzel, and G. Gréhan, "Generalized Lorenz–Mie theory for a sphere with an eccentrically located inclusion, and optical chaos," Part. Part. Syst. Charact. **18**, 190–195 (2001).
40. G. Gouesbet, S. Meunier-Guttin-Cluzel, and G. Gréhan, "Periodic orbits in Hamiltonian chaos of the annular billiard," Phys. Rev. E **65**, 016212 (2001).
41. G. Gouesbet, S. Meunier-Guttin-Cluzel, and G. Gréhan, "Morphology-dependent resonances and/or whispering gallery modes for a two-dimensional dielectric cavity with an eccentrically located circular inclusion, a Hamiltonian point of view with Hamiltonian (optical) chaos," Opt. Commun. **201**, 223–242 (2002).
42. P. T. Leung, S. W. Ng, and K. M. Pang, "Morphology-dependent resonances in dielectric spheres with many tiny inclusions," Opt. Lett. **27**, 1749–1751 (2002).

43. V. S. C. M. Rao, Gupta, and S. Dutta, "Broken azimuthal degeneracy with whispering gallery modes of microspheres," J. Opt. A Pure Appl. Opt. **7**, 279–285 (2005).
44. G. Gouesbet, "T-matrix formulation and generalized Lorenz–Mie theories in spherical coordinates," Opt. Commun. **283**, 517–521 (2010).
45. S. Stein, "Addition theorems for spherical wave functions," Quart. Appl. Math.**19**, 15–24 (1961).
46. O. R. Cruzan, "Translational addition theorems for spherical vector wave functions," Quart. Appl. Math. **20**, 33–44 (1962).
47. P. A. Bobbert and J. Vlieger, "Light scattering by a sphere on a substrate," Physica A (Amsterdam) **137**, 209–241 (1986).
48. D. W. Mackowski, "Analysis of radiative scattering from multiple sphere configurations," Proc. R. Soc. Lond. **433**, 599–614 (1991).
49. G. Gouesbet, C. Letellier, K. F. Ren, and G. Gréhan, "Discussion of two quadrature methods of evaluating beam-shape coefficients in generalized Lorenz–Mie theory," Appl. Opt. **35**, 1537–1542 (1996).
50. G. Gouesbet, G. Gréhan, and B. Maheu, "Expressions to compute the coefficients $g^m{}_n$ in the generalized Lorenz–Mie theory using finite series," J. Opt. **19**, 35 (1988).
51. K. F. Ren, G. Gouesbet, and G. Gréhan, "Integral localized approximation in generalized Lorenz–Mie theory," Appl. Opt. **37**, 4218–4225 (1998).
52. A. Doicu and T. Wriedt, "Computation of the beam-shape coefficients in the generalized Lorenz–Mie theory by using the translational addition theorem for spherical vector wave functions," Appl. Opt. **36**, 2971–2978 (1997).
53. H. Y. Zhang and Y. P. Han, "Addition theorem for the spherical vector wave functions and its application to the beam shape coefficients," J. Opt. Soc. Am. B **25**, 255–260 (2008).
54. G. Gouesbet, "Higher-order descriptions of Gaussian beams," J. Opt. **27**, 35–50 (1996).
55. J. A. Lock, "An improved Gaussian beam scattering algorithm," Appl. Opt. **34**, 559–570 (1995).
56. T. Wriedt, "The website maintained by Thomas Wriedt," http://www.scattport.org.
57. M. I. Mishchenko, J. W. Hovenier, and L. D. Travis, *Light Scattering by Nonspherical Particles: Theory, Measurements, and Applications* (Academic, 2000).
58. R. Schuh and T. Wriedt, "Computer programs for light scattering by particles with inclusions," J. Quant. Spectrosc. Radiat. Transfer **70**, 715–723 (2001).
59. P. W. Barber and S. C. Hill, *Light Scattering by Particles: Computational Methods*, Advanced Series in Applied Physics (World Scientific, 1990), Vol. 2.
60. J. A. Lock and E. A. Hovenac, "Internal caustic structure of illuminated liquid droplets," J. Opt. Soc. Am. A **8**, 1541–1552 (1991).